Properties of Nanocomposites Based on Maleate-Vinyl Ether Donor—Acceptor UV-Curable Systems

Neena Ravindran, Ankit Vora, Dean C. Webster

Department of Coatings and Polymeric Materials, Center for Nanoscale Science and Engineering, North Dakota State University, Fargo, North Dakota 58105

Received 20 September 2006; accepted 27 November 2006
DOI 10.1002/app.25971
Published online 30 May 2007 in Wiley InterScience (www.interscience.wiley.com).

ABSTRACT: UV-curable nanocomposites based on donor–acceptor crosslinking chemistry were prepared containing organically modified montmorillonites. The coatings were characterized for thermal, mechanical, and morphological properties. X-ray diffraction and transmission electron microscopy showed that nanocomposites were formed in all samples. Results showed that an increase in the percentage of clay caused an increased modulus and glass-transition temperature. It was also seen that tensile modulus showed dramatic improvement when compared with the unmodified polyester sample. Real time IR kinetic data showed that higher conversions were obtained at higher clay loadings. Pendulum hardness values and tensile modulus values showed different trends in properties depending on the combination of polymer matrix and organomodification. © 2007 Wiley Periodicals, Inc. J Appl Polym Sci 105: 3378–3390, 2007

Key words: nanocomposites; organoclay; photopolymerization; structure–property relations

INTRODUCTION

Nanocomposites are a new class of composite materials that possess structural reinforcements that are on a nanometer scale. [1] The high surface areas typical of nanoparticles result in imparting enhancement in mechanical properties that are of magnitudes higher than those obtained in regular microcomposites. Layered silicates that are commonly used in the preparation of nanocomposites belong to the structural family known as the 2 : 1 phyllosilicates. The typical feature of this family is that the crystal lattice comprises two-dimensional layers with the central layer being an octahedral alumina or magnesia fused to two tetrahedral silica layers, with the thickness of the individual layers being 1 nm and lateral dimensions being 300 Å or higher. These layers arrange themselves to form stacks and are separated by a distance related to van der Waals forces. This separation, or gap, is also referred to as the interlayer or gallery. There are charge neutralizing atoms present in the interlayer—e.g., Na^+, Li^+, Rb^+, Cs^+—and they counterbalance the negative charges generated due to isomorphic substitution within the interlayer. As such, unmodified clay is not compatible with organic polymers. However, ion-exchange reactions with cationic surfactants have the effect of overall lowering of the surface energy of the clay. [1] This exchange improves the wetting characteristics of the process and also helps to increase the interlayer spacing.

The determination and classification of nanocomposite morphology as either a phase separated, intercalated, or exfoliated structure is an important aspect of the study of structure–property relationships in polymer nanocomposites. It has been found that the rheological behavior of nanocomposites, in terms of storage modulus, is significantly different than that of unmodified materials. [2] Studies have demonstrated that mechanical properties are better in case of the clay-modified samples when compared with the unmodified samples. [2,3] Glass-transition temperature has been shown to correspondingly increase with an increase in the organoclay loading.[4] In a study on crosslinked polyester–clay nanocomposites, Bharadwaj et al. found that the morphology obtained was a mix of intercalation and exfoliation. They reported a progressively decreasing trend in properties such as tensile modulus, and loss and storage modulus with increasing clay concentration.[5] The methods used to prepare nanocomposites have been shown to influence the polyester–clay nanocomposite properties in addition to factors such as organomodification, curing conditions, etc.[6,7]

Another study found that the highest gas-barrier properties were obtained for nanocomposites with an exfoliated morphology and highest grafting density.[8] There are also a number of reports on the improved thermal stability and flame retardancy of nanocomposites.[9,10]

Correspondence to: D. C. Webster (dean.webster@ndsu.edu).

Contract grant sponsor: Defense Microelectronics Activity; contract grant numbers: DMEA90-02-C-0224, DMEA90-03-2-0303.

While there is intense research activity in the area of nanocomposites, UV-curable nanocomposites is a relatively unexplored area. UV-curable polymer nanocomposites were first reported by Zahouily et al.[11,12] Decker et al. studied bentonite–acrylate systems using real-time infrared spectroscopy (RTIR) and X-ray diffraction and concluded that nanocomposites were formed on the basis of increase in the spacing between clay layers.[13] It was also observed that the photopolymerization rate was not affected by the inclusion of the clay particles. General property improvements in UV-curable nanocomposites based on epoxy-, vinyl ether-, and acrylate-based resins have been reported.[14,15] Huimin et al. studied two different types of photopolymerization reactions and found that noncrosslinked poly(methyl methacrylate) resulted in intercalated structures, whereas crosslinking of *m*-cresol resin/*N,N*-hexa(methoxymethyl)-2,4,6-triamino-1,3,5 triazine system led to exfoliated structures.[16] Shemper et al. investigated the effect of clay on photopolymerization kinetics in the presence of hydroxylated dimethacrylate crosslinkers.[17] They also reported high rates of polymerization and high final overall conversions. Uhl et al. has reported the preparation of UV-curable nanocomposites containing organomodified clays. Some of these clays were commercially procured and other organomodified clays were prepared using an ion-exchange process.[18–20] These studies reported enhancements in Young's modulus and general improvements in mechanical and thermal properties even when the nanocomposites showed an intercalated morphology, with the incorporation of organomodified clay. It was found that while the cure time was reduced with the incorporation of clay, properties such as tensile modulus, tensile strength, glass-transition temperature increased with the clay content. Improvements in dimensional stability and adhesion were also achieved by the incorporation of clay.

Donor–acceptor systems have emerged as a viable, nonacrylate technology in the field of radiation-curable coatings. Low odor, nonirritating monomers, design flexibility, and cure characteristics that are comparable with the dominant technologies are the key features that typify this system. Free-radical-induced alternating photocopolymerization takes place when an electron-rich group is mixed with an electron deficient group.[21,22] It has been found that polymerization kinetics are affected by factors such as photoinitiator concentration, presence of oxygen, light intensity, and composition of the monomer mixture.[23–25]

In this study, UV-curable nanocomposites, based on donor–acceptor chemistry, were prepared. The purpose of the study was to understand the effect of the polymer backbone structure and the type and amount of clay on the thermal, mechanical, and morphological properties and cure characteristics of nanocomposites. This was achieved by the incorporation of clays with different surface treatment at varying percentages into different polymer-matrix compositions.

EXPERIMENTAL

Materials

All monomers used for polyester synthesis, except 1,4-cyclohexanedicarboxylic acid (1,4-CHDA), were purchased from Sigma Aldrich (Milwaukee, WI). The monomer 1,4-CHDA was obtained from Eastman Chemical Company (Kingsport, TN). Triethyleneglycol divinyl ether (TEGDVE) was provided by BASF (Ludwigshafen, Germany). Photoinitiator Darocur 1173 (2-hydroxy-2-methyl-1-phenyl-1-propanone) was supplied by CIBA (Basel, Germany). Nanomer I.31PS Onium Ion-Modified Montmorillonite, henceforth referred to as Nanomer, was provided by Nanocor (Arlington Heights, IL). Cloisite®30B and Cloisite®Na^+ were obtained from Southern Clay Products (Gonzales, TX). All chemicals were used as received without further purification.

Preparation of nanocomposites

Unsaturated polyesters were prepared using standard melt polyesterification techniques. Polyester compositions are indicated in Table I and were selected based on the findings in our earlier study.[25]

These polyesters were used to prepare nanocomposites and the methodology used is as follows. Coatings were prepared by mixing the unsaturated polyester and triethyleneglycol divinyl ether in a ratio of 1 : 1 of reactive functional groups: maleate to vinyl ether functionality. The mixture was homogenized using heat and stabilized by the addition of hydroquinone to preclude premature gelling. Clay at loadings of 1, 3, and 5 wt % was incorporated into the sample and stirred. This was followed by sonication of the sample for 8 h using an ultrasonic bath. At the end of sonication, the sample was cooled to room temperature and the photoinitiator was added. Six percent of the photoinitiator, based on the combined weight of resin, clay and reactive diluent, was added to the formulation, followed by mixing to obtain a uniform mixture.

Nomenclature

Polyesters were designated as 1, 2, 3, and 4; and their compositions are as outlined in Table I. Nanocomposites based on these polyesters are designated as polyester_type of clay_% of clay. For example, 1_Na_3 refers to a coating that contains Polyester 1 and 3% Nanomer clay. The clays are designated as follows: Nanomer: Na, Cloisite30B: Cl30B, and CloisiteNa^+:

TABLE I
Moles of Monomer Used, Final Acid Value, and Theoretical Molecular Weight for the Polyester Resins Used in This Study

Polyester	DEG	TEG	HD	TMP	CHDA	SA	PD	IPA	MA	Acid value	M_w (theo.)
1	0.8239		0.625		0.1724				1	14	772
2			1.1611	0.3871	0.3333				1	16	1034
3						0.4542	1.7566		1	20	779
4		0.4906	1.0145					0.2177	1	6	953

IPA, isophthalic acid; DEG, diethylene glycol; MA, maleic anhydride; PD, 1,5-pentanediol; HD, 1,6-hexanediol; TEG, triethylene glycol; CHDA, 1,4-cyclohexane dicarboxylic acid; SA, succinic anhydride; TMP, trimethylol propane.

ClNa+. The coating based on a particular polyester is referred to as coating followed by polyester number. For example, coating based on Polyester 1 is referred to as Coating 1.

Characterization

Cure kinetics for formulations were determined using RTIR and photodifferential scanning calorimetry (PDSC). RTIR measurements were made using a Nicolet Magna-IR 850 spectrometer with detector type DTGS KBr and scans were conducted in the transmission mode. A LESCO Super Spot MK II UV curing lamp equipped with a fiber optic light guide was the source for UV irradiation of samples. Uncured samples were spin-coated at 3000 rpm onto a KBr window. After the sample was uniformly coated, it was placed into the RTIR set-up wherein it was simultaneously exposed to IR and UV irradiation and this was performed in air. IR data collection was continued even after the UV irradiation was stopped. The sample was placed at a distance of 20 mm from the end of the fiber optic cable with a light intensity of 10 mW/cm^2 at the sample. Film thicknesses of the samples were $\sim$ 20 μm.

The rate of polymerization was calculated as per eq. (1):[26–28]

$$R_p = [M_o][((A_{1639})t_1 - (A_{1639})t_2/(t_2 - t_1))] \quad (1)$$

where $[M_o]$ is the original concentration of the vinyl ether double bonds.

Conversion was calculated using eq. (2):

$$\text{Degree of conversion} = (((A_{1639})_0 - (A_{1639})_t)/(A_{1639})_0) \times 100 \quad (2)$$

PDSC measurements were acquired using a TA Instruments Q1000 DSC outfitted with a photocalorimetric accessory. The samples were subjected to UV irradiation for 120 s at an intensity of 40 mW/cm^2 using fiber optic light guides.

These formulations were then used to prepare films. Films were deposited onto a substrate with a No. 1 Gardco bar-coater with a 4-mil clearance. Substrates used were aluminum for hardness measurement and glass for obtaining free films for DMTA and other tests. Application was followed by curing of samples under UV light until films that were nontacky to touch were obtained with the typical cure times being about 4 min. Dymax 200 EC silver lamp (UV-A, 365 nm) with an intensity of 37 mW/cm^2, measured with an International Light digital radiometer (model IL1400A), was used as the source for UV radiation. Testing on film samples were performed after allowing the samples to equilibrate at room temperature for at least 24 h.

Dynamic mechanical properties of cured films were evaluated using a dynamic mechanical thermal analyzer (DMTA 3E; Rheometric Scientific, Union, NJ). Free films of 10 mm length, 5 mm width, and 0.05–0.08 mm thickness were characterized using a frequency of 10 rad/s, heating rate of 5°C/min over a temperature range of −50 to 250°C. The geometry employed was that of rectangular tension/compression. Tan δ peaks were used to determine the T_g and crosslink density was calculated using E' value from the rubbery plateau region.

Thermogravimetric analysis was determined using a TA Instruments Q500 thermogravimetric analyzer. Samples were heated in nitrogen from 25 to 650°C, at a rate of 10°C/min.

Film hardness was measured using a BYK-Gardner pendulum hardness tester on aluminum panels and König hardness value was reported in seconds.

Tensile properties were measured using an Instron 5542. Test specimens were free-films of 5 mm width and thickness between 0.05 and 0.08 mm and at least five samples were tested to obtain an average value. The grips were set to an initial distance of 40 mm and a cross-head speed of 20.0 mm/min was applied.

X-ray powder diffraction data was collected using a Phillips PW3040 X'pert-MPD multipurpose diffractometer in Bragg-Brentano geometry (Cu Kα radiation: 1.54056 Å). The unit was equipped with a Cu monochromater, programmable divergence, scatter and receiving slits, and Soller slits on both incident and diffracted beams. Qualitative variable slit data were collected over a range of 2–40° 2θ, using a step size of 0.02 and a run time of 1 s/step.

Samples for TEM were thin cut using a diamond knife and RMC MTXL ultramicrotome. The thin sections were then placed on 400-mesh copper grids and photographed using a JEOL 100cx-II transmission electron microscope operating at 80 kV.

RESULTS AND DISCUSSION

While UV-curable polymer–clay nanocomposites have been reported based on free-radical acrylate systems and cationic epoxy systems, this study is the first where a donor–acceptor UV-curable polymer matrix was used. Thus, it was of interest to broadly explore the effects of polymer composition and organomodification of the clay on the properties of the nanocomposites formed. The unsaturated polyesters were selected on the basis of the backbone structure such that a wide range of properties could be obtained. Polyesters 1–3 have an aliphatic backbone, whereas Polyester 4 has an aromatic backbone. Polyester 1 contains a relatively higher proportion of monomers that impart greater flexibility than Polyester 2. Polyesters 1 and 2 contain cyclic monomers and Polyester 3 does not. It was expected that the variation in the composition of the backbone might result in different interactions with the clay and therefore the reinforcing effects of the coating by the clay will be different. The backbone composition affects the glass-transition temperature and this was evident in the values obtained for Polyesters 1–4, which were found to be −41.07, −36.62, −49.58, and −35.61°C, respectively.

Nanosized clays were selected on the basis of differences in surface modification and basal spacing, since it was anticipated that these differences would result in varying interactions with the polyester backbone. The surface treatment would impact the compatibility of the clay with the polymer and the difference in basal spacing would determine the extent to which the polymer can intercalate into the clay galleries. The effect of basal spacing can be explained in terms of the attraction energy ($U_{\text{attraction}}$) between two platelets of equal thickness and is given by eq. (3), derived by Stokes and Evans.[29]

$$U_{\text{attraction}} = -\frac{A_{11}}{12\pi}\left[\frac{1}{h^2} + \frac{1}{(h+2\delta)^2} - \frac{2}{(h+\delta)^2}\right] \quad (3)$$

where A_{11} is the Hamaker constant, h is separation distance between plates, and δ is platelet thickness.

As can be seen from the equation, the interaction between the platelets will decrease with square of the separation. Therefore, the choice of clays with different spacing values should result in different degrees of interaction with the polymer.

Three montmorillonite clays were selected: Nanomer (CEC = 145 meq/100 g of clay), Cloisite 30B (90 meq/100 g of clay), and Cloisite Na^+ (92.6 meq/100 g of clay). Nanomer is modified with γ-aminopropyltriethoxysilane and octadecylamine. Cloisite 30B is modified with a quaternary ammonium with substituents MeT2EtOH where Me: methyl, 2EtOH: bis-2-hydroxyethyl, and T: tallow [∼ 65% C18; ∼ 30% C16; ∼ 5% C14]; and Cloisite Na^+ is unmodified. The basal spacing 2θ values for Nanomer, Cloisite30B, and CloisiteNa^+ were found to be 3.84°, 5.12° and 8.92°, respectively. Basal spacing (*d*-spacing) values for these clays can be found in Table II.

Discernible effect of incorporation of clay in coatings

Removal of films formed on glass plates is required for tests that require free-film samples. A striking initial observation in this study was that generally the

TABLE II
X-Ray Diffraction Data for Polymer–Clay Nanocomposites

		d-spacing (nm)		
	Clay (%)	Na	Cl30B	Na+
Clay only		2.299	1.725	0.991
Coating 1	1	–[a]	–	1.611 (62.56)[b]
	3	–	–	–
	5	3.503 (52.37)	–	–
Coating 2	1	–	–	–
	3	3.503 (52.37)	1.780 (3.19)	–
	5	3.198 (39.10)	1.698 (−1.57)	1.685 (70.03)
Coating 3	1	–	–	–
	3	–	–	–
	5	–	–	1.600 (61.45)
Coating 4	1	–	–	–
	3	–	–	1.780 (79.62)
	5	3.559 (54.00)	–	1.738 (75.37)

[a] No peak observed.
[b] Values within parentheses indicate % changes.

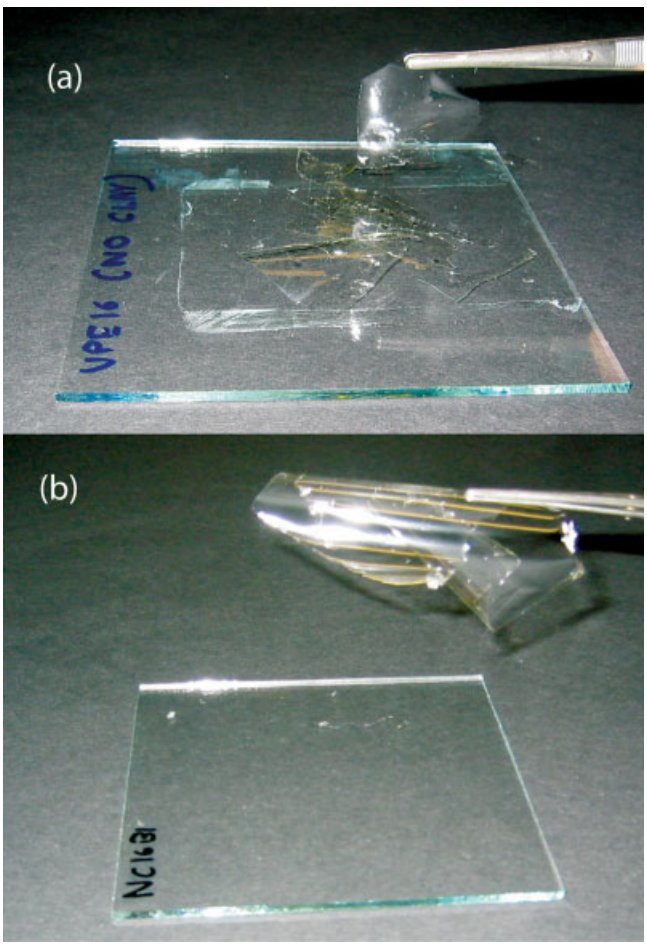

Figure 1 Picture (a) is that of unmodified sample and (b) is sample modified with 1% clay. [Color figure can be viewed in the online issue, which is available at www.interscience.wiley.com.]

unmodified coatings were brittle when compared with the coatings modified with clay and the difference is demonstrated in Figure 1. It was seen that even at a 1% clay loading, the resultant film was more ductile and mechanically robust compared with the unmodified one. This was observed in all sample sets except for Coating 4 where the films were so brittle that we were unable to peel off a film without cracking it. We attribute the enhanced flexibility to the reinforcement offered by the presence of the nanosized clay particles, which is also quantified in terms of an increase in extension at break with the incorporation of nanoparticles (discussed later). Dramatic increase in toughness has also been reported by Giannelis and coworkers in PVDF-based nanocomposites.[30] They have attributed these increases to a more efficient energy-dissipation mechanism, which delays crack formation. Due to similar sizes, nanoparticles and polymers have similar time-scales for motion. Nanoparticles act as temporary crosslinks between polymer chains, thereby providing localized regions of enhanced strength and consequently retard the growth of cavities or cracks.

Morphology of the nanocomposites

It is important to understand the exact morphological structure of the nanocomposites to enable a better understanding of the exhibited properties. X-ray diffraction and transmission electron microscopy were used to explore the morphology of the nanocomposites.

X-ray diffraction

X-ray diffraction was conducted to determine the *d*-spacing of the clay. It was expected that samples containing organically modified clays would show an increase in *d*-spacing when compared with the basal values obtained for the untreated clay. Table II contains the *d*-spacing data obtained for the four sets of coatings.

Generally, an increase in *d*-spacing is indicative of the formation of nanocomposites, since this is indicative of the polymer diffusing into the interlayer spacing of the clay. The absence of peaks may be due to exfoliation, the absence of ordering, or a higher order spacing between the layers. The data in Table II for these materials shows either an increase in *d*-spacing—when compared with the *d*-spacing obtained for the unmodified clay—or the complete absence of peaks. On the basis of these results it can be concluded that a nanocomposite was formed in all cases.

A general trend observed was that at higher clay loadings, diffraction peaks were obtained at lower 2θ values, which is an indication of intercalation. Another observation was that the nanocomposites based on Polyester 2 resulted in more samples that showed peaks when compared with those based on other polyesters. This may be attributable to the higher viscosity of Polyester 2 when compared with the others due to the presence of a trifunctional monomer, resulting in a branched structure. The higher viscosity and the branched structure could have limited the diffusion of the resin into the clay interlayer, thereby affecting the extent of increase in *d*-spacing. However, it should be noted that the *d*-spacing values obtained were still higher than that of the unmodified clay, indicating some amount of intercalation of the polymer into the interlayer.

It was also seen that the nature of the surface modification appeared to influence the final nanocomposite structure. Based on the number of samples in which peaks are absent, the highest interaction was observed in case of Cloisite 30B, followed by Nanomer, and finally Cloisite Na+. The higher interaction in case of Cloisite 30B was expected, since its surface treatment is known to have an affinity toward polar

Figure 2 TEM image of 1_Na_3.

resins.[31] Thus it was seen that the final interactions depended on the type of the polyester and the type and amount of clay.

XRD data in itself is not conclusive evidence for the formation of exfoliated nanocomposites. The absence of diffraction peaks could also be due to geometry effects or low sensitivity of the instrument at lower loadings of clay.

Transmission electron microscopy

To confirm data obtained from XRD, selected samples were analyzed using TEM and, while the data confirmed that intercalation was definitely achieved, there were also some signs of partial exfoliation. The separation of clay layers by polymer could be visually verified as seen in Figure 2. The parallel dark lines that are seen are the edges of the clay platelets. Since the discrete layers can be observed, it is concluded that the polymer has intercalated into the clay layers, but since the overall ordering of the layered silicates is still maintained, the exhibited morphology is classified as intercalated.

Photopolymerization kinetics

The kinetics of the photopolymerization of the formulations was studied using RTIR and PDSC. For RTIR measurements, the disappearance of the vinyl ether peak at 1639 cm^{-1} was monitored as a function of UV exposure time. It was seen in some samples that a higher conversion was observed in the nanocomposites when compared with the unmodified sample. Figure 3 depicts the conversion obtained for Coating 3 on 30-s UV exposure, where it is seen that the conversion for the nanocomposites is higher than that of the unmodified base polymer. This may be attributed to an increase in viscosity as cure proceeds and a resultant decrease in the termination rate. Similar rate accelerations have been observed in liquid crystalline media and a reduced mobility of the terminating radicals has been cited as the probable cause.[32] The monomeric molecules—due to their relatively high mobility—can easily diffuse to the growing chains and react, resulting in an overall higher rate of polymerization and higher conversion.

This trend was not observed in Coatings 1 and 4 as seen from the data in Table III. A slight increase in the polymerization rate has been reported by Uhl et al. and others upon the incorporation of clay in acrylate systems.[12,13,18,19] The dramatic difference observed in conversion in Coating 3 when compared with others may be attributable to the relatively low T_g of the constituent polyester which was −49.58°C (when compared with Polyesters 1, 2, and 4 with T_gs of −41.07, −36.62, and −35.61°C) and can therefore facilitate a higher degree of interaction with the clay and thereby significantly affect properties.

PhotoDSC was used to measure the heat of reaction and determine the extent of cure. The heat of reaction was obtained by integrating the area under the curve. Typical PDSC curves are as shown in Figure 4 where the maximum is denoted as H_{max}.

The rate of polymerization, R_p (from RTIR), and the heat of reaction (ΔH) (from PDSC) values with a UV exposure time of 60 s are compiled in Table III. The R_p values for Coatings 1–4 containing Nanomer clay at loadings of 1, 3, and 5% are compiled in Table III and were calculated using eqs. (1) and (2). A general observation was that the R_p was generally higher in the case of the nanocomposites.

The heat of reaction obtained in a photoDSC experiment is related to the number of reactive sites available for reaction. The experimentally obtained data was

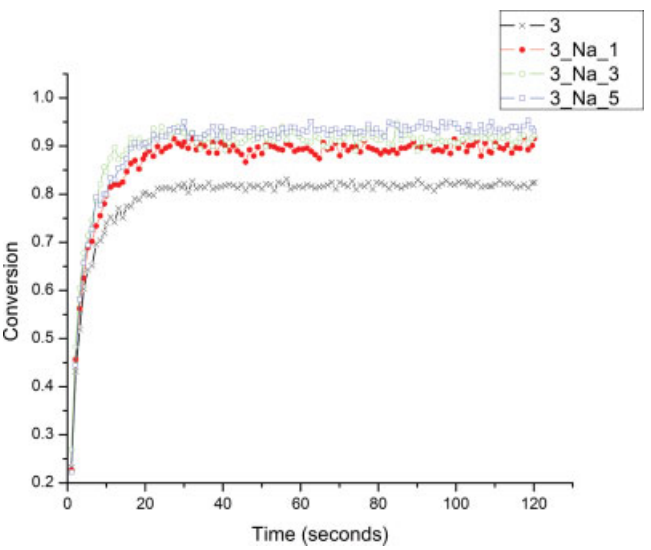

Figure 3 RTIR conversion obtained at UV exposure of 30 s for Coating 3 with Nanomer clay. [Color figure can be viewed in the online issue, which is available at www.interscience.wiley.com.]

TABLE III
Comparison of Conversion Data from RTIR and PDSC

	RTIR		PDSC	
Sample	% Conversion at 60 s	R_p (10^{-3} mol L^{-1} s^{-1})	ΔH (J g^{-1})	Conversion
1	65.70	2.52	309.3	0.95
1_Na_1	65.39	5.43	333.1	1.02
1_Na_3	65.24	3.27	330.7	1.01
1_Na_5	61.96	3.78	281.6	0.86
2	65.16	5.70	291.0	1.01
2_Na_1	69.44	9.78	260.0	0.90
2_Na_3	64.56	6.97	260.0	0.90
2_Na_5	76.88	6.17	235.9	0.82
3	75.24	9.16	333.9	1.19
3_Na_1	84.66	26.52	287.0	1.03
3_Na_3	81.87	21.52	301.1	1.08
3_Na_5	79.77	26.28	278.6	1.00
4	69.49	6.25	295.4	0.98
4_Na_1	73.73	4.07	285.8	0.96
4_Na_3	75.63	6.25	319.9	1.07
4_Na_5	70.39	9.13	288.7	0.97

used to calculate the conversion obtained and was determined as follows. The theoretical Joules/gram of the formulation was determined using eq. (4).

$$\text{Joules/gram of formulation} = BCD/M_w \qquad (4)$$

where B is number of sites/mole of monomer, C is the fraction of monomer in formula, D is Joules/mole of reactive site, and M_w is grams/mole of monomer.

This experimental heat of reaction was then divided by the theoretical, as obtained from calculations according to eq. (4), to determine the conversion in Table III.

Some general observations can be made from the data compiled in Table III. The rate of polymerization obtained from RTIR experiments was found to be higher due to the incorporation of clay. Conflicting results were obtained for conversions from RTIR and PDSC measurements. The PDSC results show that in Coating sets 1 and 4, with the introduction of clay into the system, higher conversion is obtained. Another observation is that coatings with 5% clay loading showed the lowest conversion, which was also seen in RTIR except for Coating 2. The differing results obtained from RTIR and PDSC may be due to difference in the UV intensity used in these techniques and therefore it is expected that the influence on viscosity would be different in each case. Also, RTIR was carried out in air at room temperature, whereas PDSC data was obtained under isothermal conditions at 30°C under a nitrogen purge. It would be interesting to study the trends in conversion if the experiments are run under similar conditions.

Mechanical and thermal properties

The mechanical and thermal properties are explained in terms of the following parameters: effect of backbone structure, type of clay, and amount of clay.

Dynamic mechanical thermal analysis

DMTA was used to determine the viscoelastic properties of the nanocomposite films including glass-transition temperature and crosslink density and these values are compiled in Table IV.

An increase in glass-transition temperature related to the amount of clay in clay–epoxy nanocomposites has been reported by other investigators.[33,34] It was found in this study that once the T_g reached an optimum value in a formulation containing 1% clay, no further improvements could be achieved by increasing the amount of clay. In four data sets: 1_Cl30B, 1_ClNa+, 2_Na, 2_ClNa+, the maximum T_g was obtained with 3% clay loading and further clay addition resulted in reducing the T_g. This may be attribut-

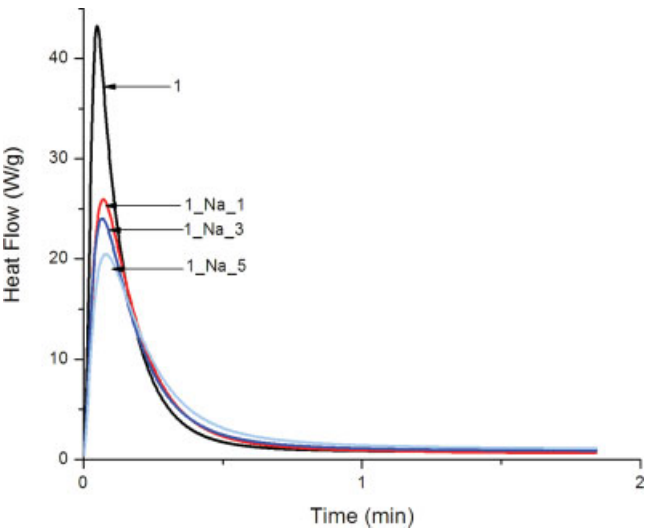

Figure 4 A typical PDSC plot. [Color figure can be viewed in the online issue, which is available at www.interscience.wiley.com.]

TABLE IV
DMTA Data

Sample	Glass-transition temperature (°C)	Crosslink density (10^{-2} mol cm^{-3})	E' (GPa) at 25°C
1	75.54	1.71	1.020
1_Na_1	84.72	1.83	1.390
1_Na_3	78.86	2.17	1.570
1_Na_5	78.10	1.91	0.990
1_Cl30B_1	81.16	1.53	1.150
1_Cl30B_3	86.44	1.35	1.070
1_Cl30B_5	78.53	1.83	1.220
1_ClNa+_1	79.90	1.75	1.240
1_ClNa+_3	93.43	1.70	1.400
1_ClNa+_5	90.15	2.09	1.680
2	59.92	1.67	0.682
2_Na_1	75.74	1.76	1.270
2_Na_3	81.02	1.80	1.420
2_Na_5	79.42	1.34	1.180
2_Cl30B_1	80.58	1.50	1.280
2_Cl30B_3	76.97	1.97	1.590
2_Cl30B_5	80.44	1.71	1.510
2_ClNa+_1	72.21	1.80	1.350
2_ClNa+_3	81.62	1.77	1.390
2_ClNa+_5	76.22	1.97	1.620
3		–	0
3_Na_1	29.24	2.24	0.711
3_Na_3	29.17	2.39	0.749
3_Na_5	25.47	3.36	0.975
3_Cl30B_1	36.52	2.31	0.868
3_Cl30B_3	27.51	2.84	0.772
3_Cl30B_5	25.52	2.88	0.780
3_ClNa+_1	68.75	1.42	0.837
3_ClNa+_3	76.79	1.92	1.070
3_ClNa+_5	81.35	1.66	1.020

able to crowding effects and the consequent reduction in the polymer–clay interactions. An unexpected observation was that a greater increase in T_g was observed with the unmodified clay. However, this may be explained by the polar nature of polyester which may have a natural affinity for the polar clay. It has been reported that there exists a close relationship between solubility parameter of the polymer and the clay morphology obtained.[35]

All other factors remaining the same, the polyester backbone played a role in the final T_g of the coating. In case of Coating 3, data for the unmodified sample could not be obtained due to the extremely brittle nature of the sample. Similarly data could not be obtained for Coating 4 since it was not possible to prepare sufficiently long samples required for testing without damaging the film. As the polymer–clay interaction increased, it was anticipated that the glass-transition temperature would increase. This was confirmed in Coatings 1 and 2 and could not be verified in case of 3 and 4 due to difficulty in sample preparation.

It was also anticipated that as the surface treatment on the clay changed, the extent of polymer–clay interaction would also change. Polyester being a polar resin, the greatest interaction was expected in formulations containing Cloisite 30B, which should effect an increase in T_g. However, T_g data showed that even when the same polyester was used, the effect on T_g varied with the difference in the type of clay. It was also seen that whereas Coatings 1 and 2 interact well with Nanomer clay, Coating 3 did not. Another striking observation was that the interaction of the unmodified clay with different backbones was comparable or better than the modified clays in all cases. The interaction was the most pronounced in case of Coating 3.

It was also seen that the polymer–clay interactions varied as the backbone changed. When Na–clay was used, interaction of similar magnitude was observed in case of Coatings 1 and 2 when compared with Coating 3. When Cl30B was used, the interactions were found to decrease in the following order of % clay content: 1 > 2 > 3. Highest interaction with Coating 3 was observed when ClNa+ was used when compared with Na and Cl30B. Therefore one can conclude that polymer backbone, type, and quantity of clay influence the T_g of nanocomposites.

It was found that generally the clay-modified coatings resulted in a higher crosslink density when compared with the unmodified coating. Also the crosslink density increased with an increase in the amount of

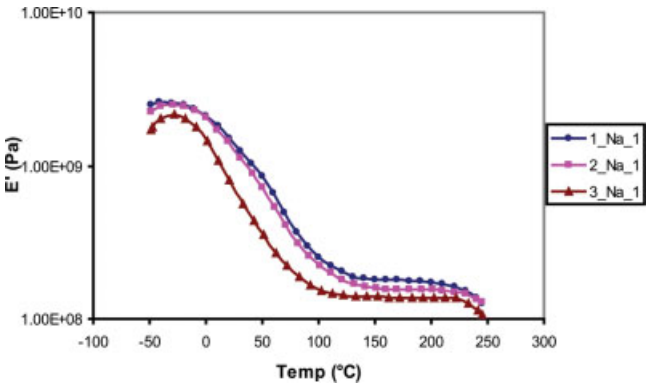

Figure 5 Effect on modulus with a change in polymer backbone structure. [Color figure can be viewed in the online issue, which is available at www.interscience.wiley.com.]

clay. Two factors can be contributing to the increase in crosslink density. First, the increase in functional group conversion on photopolymerization will lead to a higher crosslink density. In addition, physical aggregation of polymer chains onto the surface of particulates is known to occur, thereby resulting in an increase in the effective or apparent degree of crosslinking.[36]

Effect on storage modulus

The storage modulus values (E') in the viscoelastic range of −50 to 150°C were evaluated. A trend observed in all coatings except one was that a clay loading of either 3 or 5% resulted in maximum modulus at room temperature. There was no clear trend to explain the effect of backbone structure on modulus. All other factors being equal, the change in the backbone structure resulted in a change in the modulus values as seen in Figure 5, especially at lower temperatures.

Extending the observations from XRD wherein the highest interaction was observed in case of Cl30B, one can also conclude that a higher interaction with the polymer results in slightly lower modulus values as seen in Figure 6. This is also reflected in higher extension at break values for coatings containing Cl30B as seen in the following section.

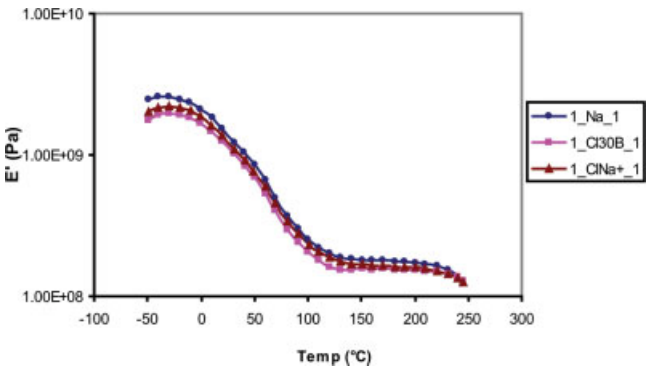

Figure 6 Effect of clay–polymer interactions on modulus values. [Color figure can be viewed in the online issue, which is available at www.interscience.wiley.com.]

Tensile properties of coatings

It was observed that the nanocomposites exhibited higher tensile modulus when compared with the unmodified samples as illustrated in Figure 7. Another trend is that with an increase in the clay loading,

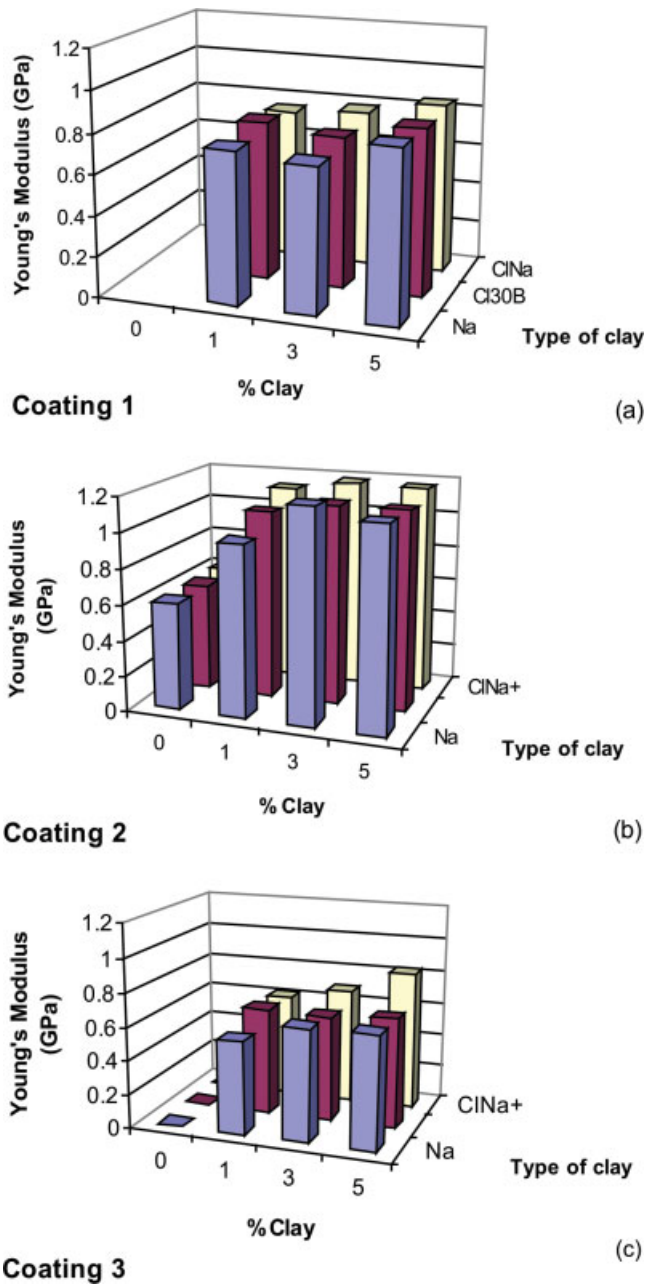

Figure 7 Plots a, b, and c depict the effect of the type and amount of clay on Young's modulus for Coatings 1, 2, and 3, respectively. [Color figure can be viewed in the online issue, which is available at www.interscience.wiley.com.]

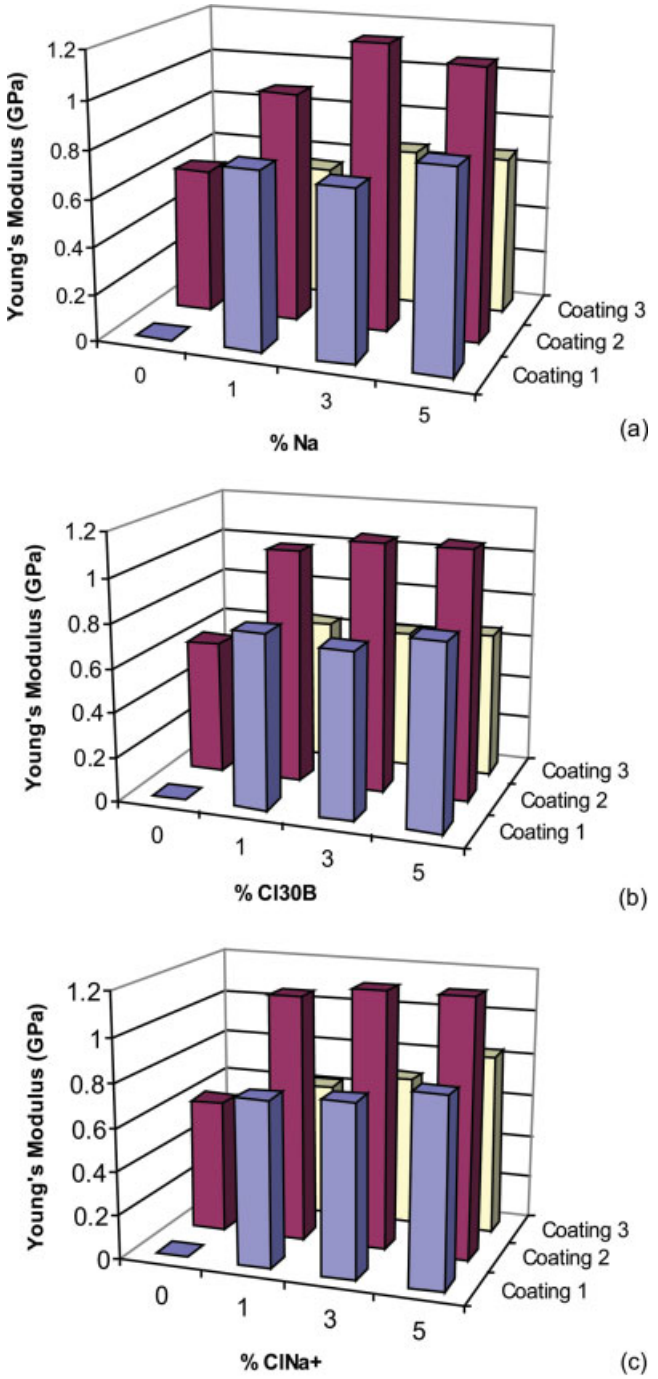

Figure 8 Plots a, b, and c depict the effect of the polymer backbone and amount of clay on Young' s modulus. [Color figure can be viewed in the online issue, which is available at www.interscience.wiley.com.]

there is a corresponding increase in Young's modulus. However, these values do not show a linear increase, and after attaining a maximum, the values begin to drop. This trend was seen in case of the different types of clay in case of Coating 2.

As seen in Figure 8, the tensile modulus was significantly affected by the change in the backbone composition of the polymer matrix. The change in the amount of clay did not seem to significantly affect the modulus and the variation in modulus as a function of clay depends on the polymer matrix and clay used. In some cases, the modulus reaches a maximum at 1 or 3% clay loading. This is perhaps due to the additional clay not being well dispersed into the polymer matrix.

From the data compiled in Table V, it can be concluded that generally the incorporation of clay into a formulation results in an increase in elongation and modulus. The improvement in modulus with the incorporation of clay particles is also substantiated by the DMTA modulus values at room temperature as seen in Table IV. It is also known that filler particles reduce mobility of polymer chain and result in a higher Young's modulus value.[37] Our observations were similar and it is illustrated in Figures 7 and 8 and Table V which contains the data for extension at break. It is seen that the backbone structure had a greater impact on modulus values than the type or amount of clay. The polyester with the most flexible backbone based on T_g values, Coating 3 was found to exhibit the lowest modulus value and the highest T_g

TABLE V
Young's Modulus and Extension at Break Values for Different Formulations

Sample	Ext. at break (mm)
1	Could not be measured
1_Na_1	0.56
1_Na_3	0.61
1_Na_5	0.71
1_Cl30B_1	0.77
1_Cl30B_3	0.75
1_Cl30B_5	0.87
1_ClNa+_1	0.63
1_ClNa+_3	0.62
1_ClNa+_5	0.97
2	0.53
2_Na_1	0.6
2_Na_3	0.47
2_Na_5	0.44
2_Cl30B_1	0.69
2_Cl30B_3	0.5
2_Cl30B_5	0.58
2_ClNa+_1	0.42
2_ClNa+_3	0.46
2_ClNa+_5	0.37
3	Could not be measured
3_Na_1	0.71
3_Na_3	0.54
3_Na_5	0.6
3_Cl30B_1	0.74
3_Cl30B_3	0.8
3_Cl30B_5	1.06
3_ClNa+_1	0.5
3_ClNa+_3	0.54
3_ClNa+_5	0.59

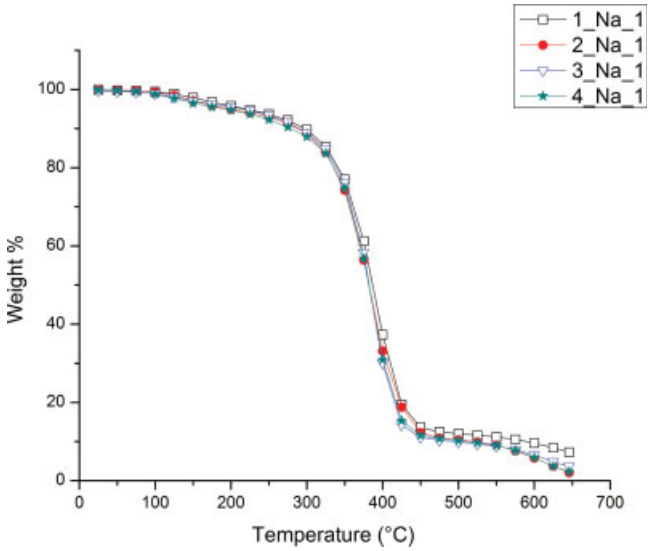

Figure 9 Effect of backbone structure on thermal stability. [Color figure can be viewed in the online issue, which is available at www.interscience.wiley.com.]

was found to have higher modulus values. Similar trends were observed in case of extension at break values.

Thermogravimetric analysis

Thermogravimetric analysis of the samples revealed the following trends. While the onset of decomposition was similar for all of the samples, at higher temperatures, slight differences are observed in the TGA plots (Fig. 9).

It was also observed that the modified samples had a higher amount of char than the unmodified sam-

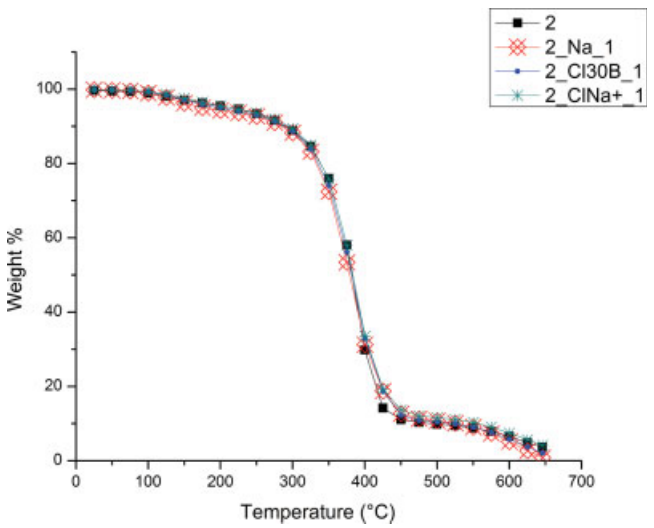

Figure 10 Effect of different clay type on thermal stability. [Color figure can be viewed in the online issue, which is available at www.interscience.wiley.com.]

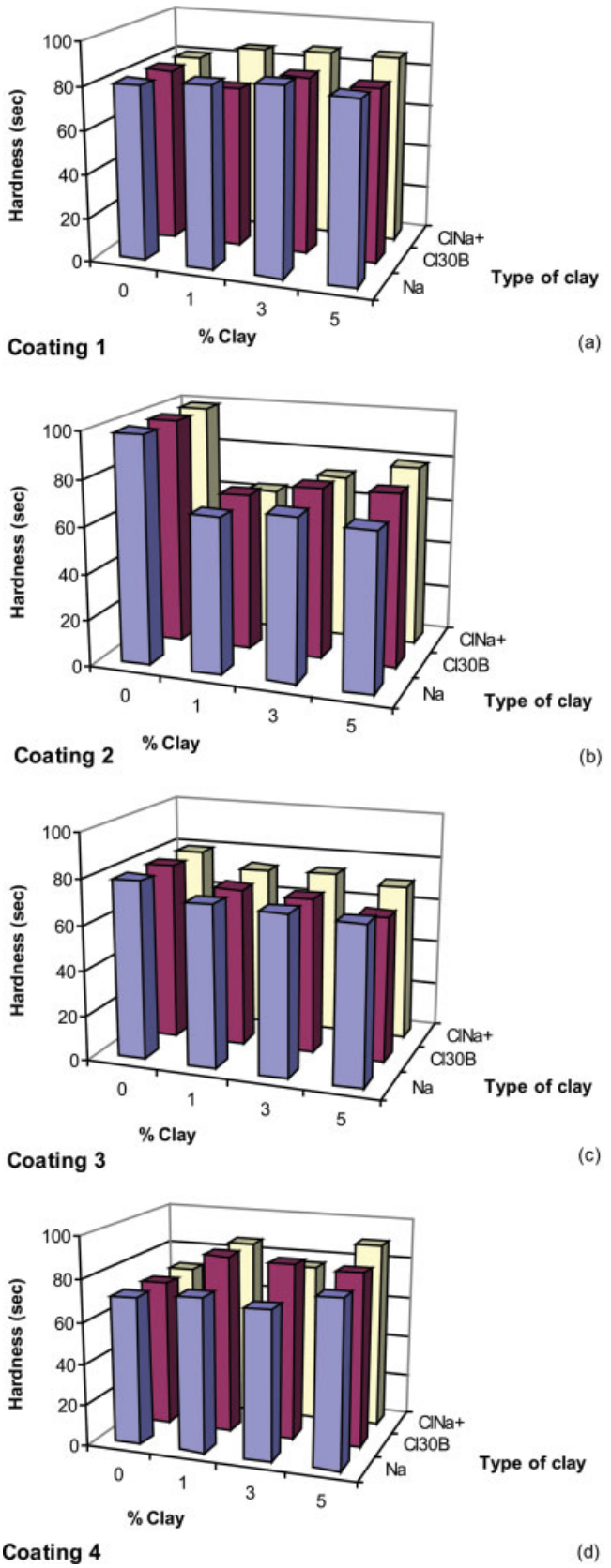

Figure 11 Plots a, b, c, and d depict the effect of the type and amount of clay on hardness of Coatings 1, 2, 3, and 4, respectively. [Color figure can be viewed in the online issue, which is available at www.interscience.wiley.com.]

ples, as illustrated in Figure 10. The increase in char in case of the modified samples can be attributed to the presence of clay, which remains at the end of the heating cycle. All coatings demonstrated good thermal stability up to a temperature of 350°C. However, there were no significant changes in thermal stability due to the incorporation of nanoparticles.

König pendulum hardness

König pendulum hardness was determined for the nanocomposites and compared with the values obtained for the unmodified coatings as illustrated in Figure 11. In the case of nanocomposites based on 2 and 3, the pendulum hardness values were higher in case of unmodified coatings. However, in case of Coatings 1 and 4, enhancement in hardness was observed when clay was introduced into the system. There were three different trends observed in the pendulum hardness values. The first trend was that as the percent clay increased in the composition the hardness increased. The second trend was that as the % clay increased the hardness decreased. The third trend was in a given set of coatings, e.g., 4_Na_1, 4_Na_3, 4_Na_5, the hardness value for 3% clay increased and there were other sets wherein there was a decrease in hardness value at 3%. As in the case of the tensile modulus data, this could be due to crowding where additional clay is unable to be well-dispersed into the polymer matrix. Although no clear trends are discernible, it is very evident that either the individual contributions of or a combination of the type of polymer backbone, type of clay, and amount of clay has an impact on the final properties. Further studies are warranted to delineate the exact contributions of the aforementioned factors.

CONCLUSIONS

Enhancements in cure characteristics, thermal, and mechanical properties were observed in UV-curable nanocomposites based on donor–acceptor chemistry. Based on the XRD and TEM results it could be concluded that intercalated nanocomposites were formed in all cases. It was seen that the type of polyester and clay were the major factors influencing the final nanocomposite structure. An interaction of a higher magnitude was observed in case of coatings containing clay Cl30B. Cure characteristics, tensile properties, hardness, and glass-transition temperature were found to vary as function of type and percentage of clay. A dramatic increase in polymerization rate was observed in two coating sets after incorporation of clay, attributable to the autoacceleration effect. It was found that the coatings without clay were brittle and incorporation of even 1% clay significantly improved the ductility. Increase in glass-transition temperature and tensile modulus were observed after incorporation of clay. No significant changes were observed in case of thermal stability and hardness due to the incorporation of clay nanoparticles.

We thank Siva Prashant Davuluri and Scott Payne for assistance with transmission electron microscopy of samples.

References

1. Alexandre, M.; Dubois, P. Mater Sci Eng R 2000, 28, 15.
2. Inceoglu, A. B.; Yilmazer, U. Polym Eng Sci 2003, 43, 661.
3. Kornmann, X.; Berglund, L. A.; Sterte, J. Polym Eng Sci 1998, 38, 351.
4. Laus, M.; Camerani, M.; Lelli, M.; Sparnacci, K.; Sandrolini, F.; Francescangeli, O. J Mater Sci 1998, 33, 2883.
5. Bharadwaj, R. K.; Mehrabi, A. R.; Hamilton, C.; Trujillo, C.; Murga, M.; Fan, R.; Chavira, A.; Thompson, A. K. Polymer 2002, 43, 3699.
6. Suh, D. J.; Lim, Y. T.; Park, O. O. Polymer 2000, 41, 8557.
7. Mironi-Harpaz, I.; Narkis, M.; Siegmann, A. Polym Sci Eng 2005, 45, 174.
8. Gain, O.; Espuche, E.; Pollet, E.; Alexandre, M.; Dubois, P. J Polym Sci Part B: Polym Phys 2005, 43, 205.
9. Zhu, J.; Morgan, A. B.; Lamelas, F. J.; Wilkie, C. A. Chem Mater 2001, 13, 3774.
10. Beyer, G. Plast Addit Compd 2002, 4, 22.
11. Zahouily, K.; Benfarhi, S.; Bendaikha, T.; Baron, J.; Decker, C. Proc Radtech Eur 2001, 583.
12. Zahouily, K.; Decker, C.; Benfarhi, S.; Baron, J. Technical Conference Proceedings, Radtech 2002, The Premier UV/EB Conference and Exhibition, Indianapolis, IN, April 28–May 1, 2002, p 309.
13. Decker, C.; Zahouily, K.; Keller, L.; Benfarhi, S.; Bendaikha, T.; Baron, J. J Mater Sci 2002, 37, 4831.
14. Benfarhi, S.; Decker, C.; Keller, L.; Zahouily, K. Eur Polym J 2004, 40, 493.
15. Keller, L.; Decker, C.; Zahouily, K.; Benfarhi, S.; Le Meins, J. M.; Miehe-Brendle, J. Polymer 2004, 45, 7437.
16. Huimin, W.; Minghua, M.; Yongcai, J.; Qingshan, L.; Xiaohong, Z.; Shikang, W. Polym Int 2001, 51, 7.
17. Shemper, B. S.; Morizur, J.-F.; Alirol, M.; Domenech, A.; Hulin, V.; Mathias, L. J. J Appl Polym Sci 2004, 93, 1252.
18. Uhl, F. M.; Davuluri, S. P.; Wong, S. C.; Webster, D. C. Chem Mater 2004, 16, 1135.
19. Uhl, F. M.; Davuluri, S. P.; Wong, S.-C.; Webster, D. C. Polymer 2005, 45, 6187.
20. Uhl, F. M.; Hinderliter, B. R.; Davuluri, S. P.; Croll, S. G.; Wong, S. C.; Webster, D. C. Presented at Technical Conference Proceedings—UV and EB Technology Expo and Conference, Charlotte, NC, May 2–5, 2004; p 610.
21. Lee, C.; Hall, H. K., Jr. Macromolecules 1989, 22, 25.
22. Jonsson, S.; Sundell, P.; Hultgren, J.; Sheng, D.; Hoyle, C. E. Prog Org Coat 1996, 27, 107.
23. Zhang, L.; Liu, L.; Chen, Y. J Appl Polym Sci 1999, 74, 3541.
24. Decker, C.; Decker, D. Polymer 1997, 38, 2229.
25. Ravindran, N.; Vora, A.; Webster, D. C. Presented at the Technical Conference Proceedings—UV and EB Technology Expo and Conference, Charlotte, NC, May 2–5, 2004; p 148.
26. Stowe, F. S.; Lieberman, R. A. J Radiat Curing 1987, 14, 10.
27. Decker, C.; Moussa, K. Makromol Chem 1988, 189, 2381.

28. Decker, C.; Moussa, K.; Makromol Chem Rapid Commun 1990, 11, 159.
29. Stokes, R. J.; Evans, D. F. Fundamentals of Interfacial Engineering; Wiley-VCH: New York, 1997.
30. Shah, D.; Maiti, P.; Gunn, E.; Schmidt, D. F.; Jiang, D. D.; Batt, C. A.; Giannelis, E. P. Adv Mater 2004, 16, 1173.
31. Lee, K. M.; Han, C. D. Macromolecules 2003, 36, 7165.
32. Hoyle, C. E.; Chawla, C. P.; Kang, D.; Griffin, A. C. Macromolecules 1993, 26, 758.
33. Wang, M. S.; Pinnavaia, T. J. Chem Mater 1994, 6, 468.
34. Lan, T.; Kaviratna, D.; Pinnavaia, T. J.; Chem Mater 1995, 17, 2144.
35. Jang, B. N.; Wang, D.; Wilkie, C. A. Macromolecules 2005, 38, 6533.
36. Mark, J. E.; Erman, B. Rubberlike Elasticity: A Molecular Primer; Wiley: New York, 1988.
37. Elias, H.-G. Macromolecules: Synthesis, Materials, and Technology, 2nd Edition; Plenum Press: New York, 1984.